Journal of Electrochemistry

Volume 20
Issue 6 *Special Issue of Bioelectroanalyical Chemistry (Editor: Professor XIA Xing-hua)*

2014-12-28

Comparison in Factors Affecting Electrochemical Properties of Thermal-Reduced Graphene Oxide for Supercapacitors

Peng XIAO

Da-Hui WANG
School of Material Science and Engineering, Lanzhou University of Technology, Lanzhou 730050, China;, wangdh@lut.cn

Jun-Wei LANG
Laboratory of Clean Energy Chemistry and Materials, Lanzhou Institute of Chemical Physics, Chinese Academy of Sciences, Lanzhou 730000, China;, jwlang@licp.cas.cn

Recommended Citation
Peng XIAO, Da-Hui WANG, Jun-Wei LANG. Comparison in Factors Affecting Electrochemical Properties of Thermal-Reduced Graphene Oxide for Supercapacitors[J]. *Journal of Electrochemistry*, 2014 , 20(6): 553-562.
DOI: 10.13208/j.electrochem.140213
Available at: https://jelectrochem.xmu.edu.cn/journal/vol20/iss6/9

DOI: 10.13208/j.electrochem.140213 **Artical ID**:1006-3471(2014)06-0553-10
Cite this: *J. Electrochem.* **2014**, *20*(6): 553-562 **Http**://electrochem.xmu.edu.cn

Comparison in Factors Affecting Electrochemical Properties of Thermal-Reduced Graphene Oxide for Supercapacitors

XIAO Peng[1,2], WANG Da-Hui[1*], LANG Jun-Wei[2*]
(1. *School of Material Science and Engineering, Lanzhou University of Technology, Lanzhou* 730050, *China*;
2. *Laboratory of Clean Energy Chemistry and Materials, Lanzhou Institute of Chemical Physics, Chinese Academy of Sciences, Lanzhou* 730000, *China*)

Abstract: In this paper, thermal-reduced graphene oxide (T-RGO) materials are synthesized by modified Hummer's method, followed by thermal reduction under argon atmosphere at different temperatures. Electrochemical investigations show that, for T-RGO electrodes, good electrical conductivity is necessary and the surface functional groups play more significant role than the specific surface area in determining the electrochemical capacitance. The T-RGO obtained at 900 ºC (T-RGO_{900}) with a relatively high Brunauer-Emmett-Teller (BET) surface area (314 $m^2 \cdot g^{-1}$) and a high electrical conductivity (2421 $S \cdot m^{-1}$) shows a low specific capacitance of 56 $F \cdot g^{-1}$. In comparison, the T-RGO obtained at 300 ºC (T-RGO_{300}) with a relatively low BET surface area (18.8 $m^2 \cdot g^{-1}$) and an electrical conductivity (574 $S \cdot m^{-1}$) provides the largest specific capacitance of 281 $F \cdot g^{-1}$. The large specific capacitance of T-RGO_{300} results from the simultaneous contributions of the electrochemical double-layer capacitance and the pseudo-capacitance obtained from the oxygenated groups on the T-RGO surfaces. Therefore, it probably gives a new insight for designing and synthesizing graphene-based electrode materials for supercapacitors and other energy-storage devices.

Key words: graphene; pseudo-capacitance; supercapacitor; surface functional groups; thermal reduction
CLC Number: O646 **Document Code**: A

Environmentally friendly, high-performance energy-storage system is crucial for the survival of our civilization[1-2]. As a kind of energy storage/conversion devices, supercapacitors exhibit much higher energy density than conventional capacitors, greater power density and longer cycling life than common batteries. However, supercapacitors are still not capable of delivering high energy densities comparable to those of lithium ion batteries and fuel cells[3-6]. Thus, present supercapacitor developments should be oriented towards the increasing of the energy density to be close to or even beyond that of batteries as well as lowering fabrication costs.

Currently, various carbonaceous materials such as carbon black, activated carbon, carbon nanotubes, mesoporous carbon, carbon aerogels and carbon nanofibers have been extensively studied for supercapacitors because of their large surface areas, good electronic conductivities, stable physicochemical properties and long cycle life. Their charge storage mechanism is built upon the formation of electrochemical double layer capacitances (EDLCs) at the electrode/electrolyte interfaces[7].

When carbon atoms are tightly packed into a two-dimensional sp^2 carbon lattice, they form a single atom thick allotrope of carbon: graphene[8]. Graphene is proposed as the next generation electrode material for supercapacitors owing to its chemical stability, excellent electrical conductivity and exceptionally large theoretical surface area (over 2600 $m^2 \cdot g^{-1}$)[9].

Received: 2014-02-13 , Revised: 2014-05-06 *Corresponding author, Tel: (86-931)2973563 ; (86-931)4968055 , E-mail: wangdh@lut.cn; jwlang@licp.cas.cn
This work was supported by The Top Hundred Talents Program of the Chinese Academy of Sciences and National Natural Science Foundations of China (No. 51005225, No. 21203223)

However, like most nanomaterials, graphene nanosheets (GNSs) are also likely to form irreversible agglomerates through the van der Waals interactions during the drying process. In such case, the surface area of as-prepared GNSs is usually much lower than the theoretical one and the capacitance is much lower than the anticipated value[10].

As we know, besides surface area, pore characteristics and electrical conductivity, chemical contribution also plays an important role in determining the capacitive performance of porous carbon materials[11]. Similarly, the amount of stored energy of graphene-based supercapacitors can be obviously enhanced through pseudo-faradic reactions of active groups on the surfaces of graphene. These surface functional groups modify the electron donor/acceptor properties of graphene layers and affect the charging of the electrical double layer, as a result of a pseudo-capacitance effect[12].

Up to date, many approaches have been developed to prepare GNSs for supercapacitor electrodes. Among them, liquid-phase chemical conversion is considered to be the most effective way for large-scale and low-cost preparation of GNSs. In this route, graphite oxide (GO) is generally prepared from graphite and then converted to graphene via sonication exfoliation followed by chemical reduction using hydrazine[13]. In view of the toxicity and combustibility of hydrazine, thermal reduction is alternative efficient method to obtain graphene. Also, the high temperature thermal reduction (normally above 800 ℃) associates the exfoliation of GNSs and removal of oxygen-containing groups, resulting in the increase of both the surface area and the electrical conductivity of the final GNS products, which would be in favor of the EDLCs improvement of GNSs[14]. However, the high temperature treatment is a high energy-consuming process, which is not propitious for practical application. More importantly, the removal of oxygen-containing groups would eliminate the pseudo-capacitance contribution. So, a question arises, which does play the most significant role in determining the electrochemical capacitance of thermal-reduced graphene oxide (T-RGO)? Is surface area, electrical conductivity or surface functional groups? However, there is no systematic study on this issue to date. Therefore, it is very necessary to analyze the constraining effect each other and to find the optimal reduction temperature of T-RGO for supercapacitors.

In this work, we study the differences in surface area, electrical conductivity and surface chemical components of GO and T-RGO prepared at low and high temperatures, respectively, and the differences in their electrochemical capacitive properties. Our results indicate that the oxygen-containing functional groups on T-RGO surfaces play the most important role on capacitance contribution. The $T\text{-}RGO_{300}$ with a low specific surface area possesses the largest specific capacitance of 281 $F \cdot g^{-1}$ in aqueous KOH electrolyte. Taking its large capacitance and low energy-consumption into consideration, the T-RGO prepared at low temperature may be an attractive candidate as an electrode material for supercapacitors. Also, this work probably gives a new insight for designing and synthesizing electrode materials of supercapacitors and other energy-storage devices.

1 Experimental

1.1 Preparations of GO and T-RGO

GO was synthesized from natural graphite powders by a modified Hummer's method according to the literature[15]. After dialysis for one month to remove remaining impurities, exfoliation was carried out with the aid of poly-style sonication at 500 W for 120 min. Then, the resulting mixture was dried at 80 ℃ in air to get GO powders.

The dried GO powders were thermally reduced at 200 ℃, 300 ℃, 400 ℃, and 900 ℃ for 3 h under argon atmosphere with the same heating rate of 2 $℃ \cdot min^{-1}$. The obtained samples were denoted as $T\text{-}RGO_{200}$, $T\text{-}RGO_{300}$, $T\text{-}RGO_{400}$, and $T\text{-}RGO_{900}$, respectively.

1.2 Structural Characterizations

The thermal property of GO was conducted with a thermogravimetric analysis (TGA-DSA 2960, TA

Instruments). The weight loss of sample was monitored from room temperature to 900 ℃ at a heating rate of 10 ℃·min^{-1} in argon atmosphere. The morphology and crystallite structure of the as-obtained products were investigated using a field emission scanning electron microscope (FESEM, JSM-6701F) and a X-ray diffraction (XRD, X'Pert Pro, Philips) using Cu K_α radiation. Nitrogen adsorption-desorption isotherm measurements were performed on a Micromeritics ASAP 2020 volumetric adsorption analyzer at 77 K to analyze the surface area and pore structure of the samples. The Brunauer-Emmett-Teller (BET) method was utilized to calculate the specific surface area of each sample. The surface chemical compositions of the GO, T-RGO$_{300}$ and T-RGO$_{900}$ samples were analyzed on a Perkin-Elmer PHI-5702 multifunctional X-ray photoelectron spectroscope (XPS, physical Electronics, USA) using Al K_α radiation of 1486.6 eV as the excitation source. The electrical conductivity of the GO, T-RGO$_{300}$ and T-RGO$_{900}$ samples was measured by a four-probe method. Before the measurement, powdery samples need to be pressed into tablet-like shape with a 10 MPa pressure.

1.3 Electrode Preparations and Electrochemical Measurements

The working electrodes were prepared according to the method reported previously[16]. Typically, 80% (by mass, the same below) of electroactive material was mixed with 7.5% of acetylene black (> 99.9%) and 7.5% of conducting graphite in an agate mortar until a homogeneous black powder was obtained. To this mixture, 5% of poly(tetrafluoroethylene) was added with a few drops of ethanol. After briefly allowing the solvent to evaporate, the resulting paste was pressed at 10 MPa to nickel foam (thickness: 1.8 mm; pore density: 420 g·m^{-2}). The electrode assembly was dried for 16 h at 80 ℃ in air. Each electrode contained about 8 mg of electroactive material had a geometric surface area of about 1 cm^2.

The electrochemical measurements of each as-prepared electrode were carried out using an electrochemical working station (CHI660D, Shanghai, China) in a three-electrode system in 2 mol·L^{-1} KOH electrolyte at room temperature. A platinum gauze electrode and a saturated calomel electrode (SCE) served as the counter electrode and the reference electrode, respectively. The cyclic voltammetry (CV) measurements were conducted at different scan rates ranging from 10 to 200 mV·s^{-1}. Electrochemical impedance spectroscopy (EIS) data were recorded from 10 kHz to 100 MHz with an amplitude of ±5 mV, the potential for the electrodes was -0.1 V vs. SCE. Galvanostatic charge/discharge measurements were run on at different current densities ranging from 0.5 to 10 A·g^{-1}. The corresponding specific capacitance was calculated from:

$$C = I/[(\mathrm{d}E/\mathrm{d}t)\times m] \approx I/[(\Delta E/\Delta t)\times m]\ (\mathrm{F\cdot g^{-1}}) \quad (1)$$

where C is the specific capacitance, I is the constant discharging current, dE/dt indicates the slope of the discharging curves, and m is the mass of the corresponding electrode material.

2 Results and Discussion

2.1 Microstructures

To evaluate the thermal stability of GO, TGA was performed in argon atmosphere to characterize the mass loss with the temperature. As shown in Fig. 1, an abrupt mass loss of 51% is observed in the temperature range of 70 ~ 300 ℃, which indicates that most of oxygen-containing functional groups bonded to graphene planes are removed in this temperature range[17]. A slow and continuous weight loss still occurs above 300 ℃, which is attributed to the removal of the residual oxygen-containing groups on the surfaces of GO.

The surface chemical components and the atomic concentrations of GO and T-RGO were evaluated using XPS analyses, and the high-resolution C1s XPS spectra of GO, T-RGO$_{300}$ and T-RGO$_{900}$ are present in Fig. 2. Also, the corresponding analytic results are summarized in Tab. 1. The C1s XPS spectrum of GO (Fig. 2A) clearly indicates a considerable degree of oxidation with four different peaks which correspond to C═C bonds (284.4 eV), C—O bonds (286.3 eV), C═O bonds (287.5 eV), and O—C═O bonds (289.0 eV), respectively. After thermal reduction, the intensi-

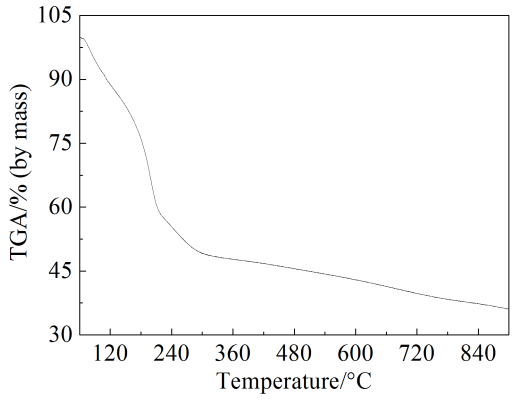

Fig. 1 The TGA curve of GO in argon atmosphere

ty of C=C bond increases, but the intensities of all oxygen-containing bonds decrease obviously, which reveals that most oxygen containing functional groups have been removed after reduction. Based on the TGA and XPS results, we can draw the conclusion that the deoxygenation degree of T-RGO gradually increases with the increase of the reduction temperature. Therefore, T-RGO$_{300}$ contains more residual oxygen-containing groups than T-RGO$_{900}$.

The XRD patterns of GO, T-RGO$_{300}$ and T-RGO$_{900}$ are shown in Fig. 3. For the GO sample, a sharp peak at 12° corresponds to the (002) reflection of stacked GO sheets, suggesting the considerable oxidation of the starting graphite and the introduction of oxygen-containing groups on GO sheets. After thermal reduction, the sharp peak around 12° at the XRD patterns is fully disappeared, indicating that oxygen-containing groups on GO sheets are removed during the thermal reduction. For T-RGO$_{300}$, a broad diffraction peak at 23.1° and a small diffraction peak at 42.8° can be attributed to the graphite-like structure (002) and (100), respectively. The small shift of (002) indicates that some residual oxygen-containing functional groups may be present between the graphene layers. Compared with T-RGO$_{300}$, T-RGO$_{900}$ displays a much wider peak centered at 25°, revealing that the efficient exfoliation of GO and the formation of single- or few-layered GNSs.

The SEM images of the GO, T-RGO$_{300}$ and T-RGO$_{900}$ products are shown in Fig. 4. It can be observed that both GO and T-RGO$_{300}$ are not efficiently exfoliated and tend to form dense agglomerates in dry state. It is owing to the strong van der Waals interactions between the layers of GO. In addition, some

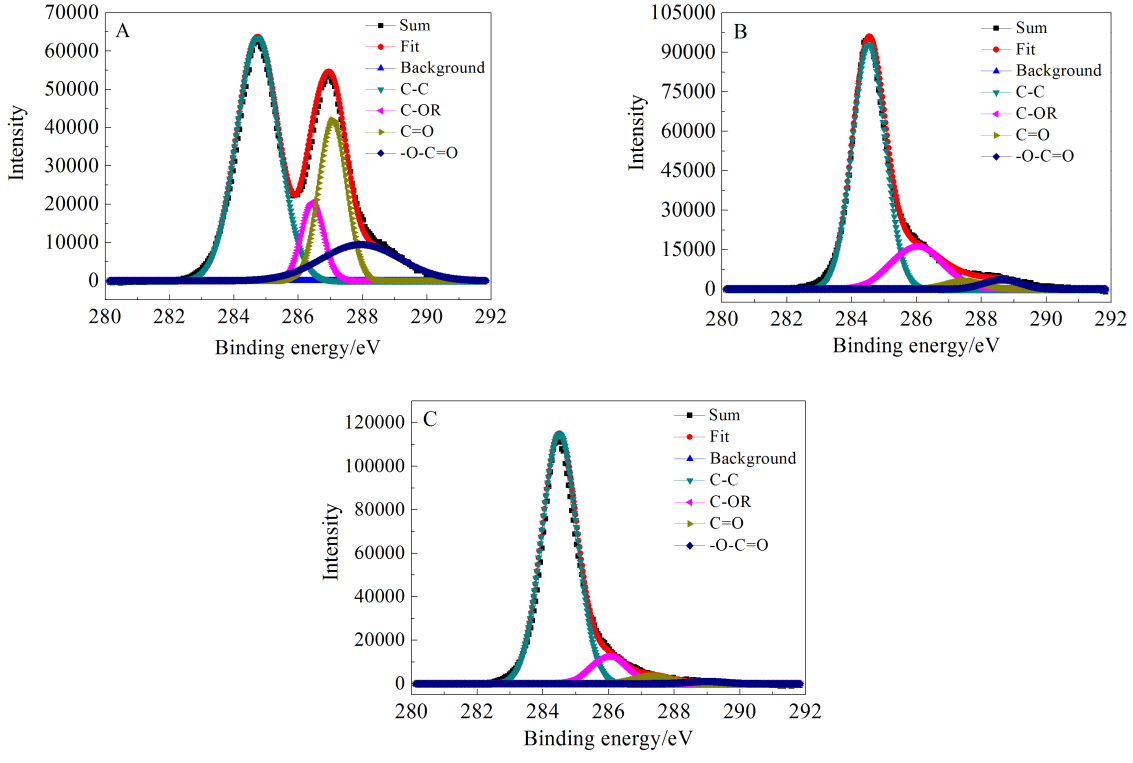

Fig. 2 C1s XPS spectra of the GO (A), the T-RGO$_{300}$ (B) and the T-RGO$_{900}$ (C) samples

Tab. 1 XPS surface characterization of the GO and the T-RGO samples

Sample	C at.%	O at.%	N at.%	C═C (C—C) at.% (284.4 eV)	C—OR at.% (286.3 ± 0.2 eV)	C═O at.% (287.5 ± 0.2 eV)	—O—C═O at.% (289.0 ± 0.2 eV)
GO	70.6	29.4	0	36.3	6.9	16.5	10
$T\text{-}RGO_{300}$	88	12	0	65.5	17.2	2.4	2.8
$T\text{-}RGO_{900}$	96	4	0	83.2	9.3	2.7	0.8

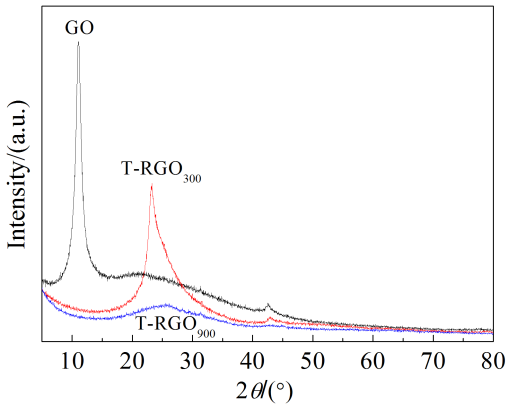

Fig. 3 The XRD patterns of the GO, $T\text{-}RGO_{300}$ and $T\text{-}RGO_{900}$ samples

layer-like structures can be observed at the edges of the agglomerates. In comparison, SEM image of $T\text{-}RGO_{900}$ shows catachrestic ultrathin sheets, which reveals that most of GO are efficiently exfoliated at 900 ℃.

Tab. 2 summarizes the textural properties of the GO, $T\text{-}RGO_{300}$ and $T\text{-}RGO_{900}$ samples. The BET surface area of GO is only 17.7 $m^2 \cdot g^{-1}$. After thermal reduction at 300 ℃, the BET surface area and pore volume increase slightly. It suggests that $T\text{-}RGO_{300}$ still remains stacked graphitic layer structure, which is in agreement with the result of SEM. We believe that such a low temperature is able to drive most oxygen-containing groups to flee from the planar GO sheets, but is not enough to exfoliate GO layers under an atmospheric pressure. As shown in Tab. 2, for $T\text{-}RGO_{900}$, the BET surface area is 313 $m^2 \cdot g^{-1}$ and the pore volume is 1.67 $cm^3 \cdot g^{-1}$. The values are much larger than those of GO and $T\text{-}RGO_{300}$, indicating the realization of an efficient expansion-exfoliation at 900 ℃. In addition, the electrical conductivity of the GO, $T\text{-}RGO_{300}$ and $T\text{-}RGO_{900}$ samples was measured by a standard four probe method, and the results are shown in Tab. 2 as well. The conductivity of GO is 1.2×10^{-3} $S \cdot m^{-1}$, while the conductivity values of $T\text{-}RGO_{300}$ and $T\text{-}RGO_{900}$ are 574 and 2421 $S \cdot m^{-1}$, respectively.

2.2 Electrochemical Properties

CV and chronopotentiometry measurements were employed to evaluate the electrochemical properties and to calculate the specific capacitances of as-prepared electrodes. Fig. 5A shows the CV curves of the GO, $T\text{-}RGO_{300}$ and the $T\text{-}RGO_{900}$ electrodes at the scan rate of 10 $mV \cdot s^{-1}$ between -1.0 and 0 V (vs. SCE) in 2 $mol \cdot L^{-1}$ KOH aqueous electrolyte. It can be seen that the CV curve of the $T\text{-}RGO_{900}$ electrode is close to the ideal rectangular shape, which indi-

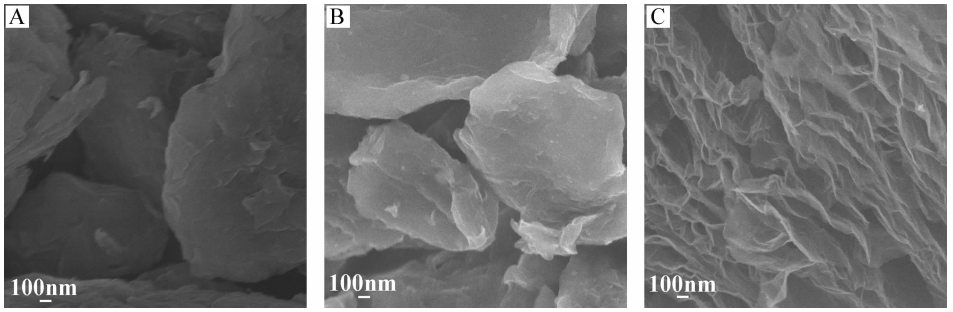

Fig. 4 SEM images of GO (A), $T\text{-}RGO_{300}$ (B) and $T\text{-}RGO_{900}$ (C) samples

Tab. 2 Specific surface areas, pore volumes, specific capacitances and electrical conductivity of GO and T-RGO samples

Sample	BET specific surface area/ ($m^2 \cdot g^{-1}$)	BJH pore volume/ ($cm^3 \cdot g^{-1}$)	Specific capacitance/ ($F \cdot g^{-1}$)	Electrical conductivity/ ($S \cdot m^{-1}$)
O	17.7	0.03	53	1.2×10^{-3}
$T\text{-}RGO_{300}$	18.8	0.07	281	574
$T\text{-}RGO_{900}$	313.8	1.67	56	2421

cates that the electrochemical behavior based on $T\text{-}RGO_{900}$ is more like an ideal EDLC. Due to the very poor electrical conductivity (1.2×10^{-3} S·m^{-1}) of GO materials, any additional pseudo-capacitance can be seen and very obvious polarization appears in the CV curve of the GO electrode at the two edges of potential window. However, the CV curve of the $T\text{-}RGO_{300}$ electrode deviates from idealized double-layer behaviors with a pair of broad, superimposed and reversible faradaic surface redox reactions, behaving as a pseudo-capacitor. It is attributed to redox reactions of the O (pyrone-like) functional groups on the surface of the $T\text{-}RGO_{300}$. Moreover, it is clear that the $T\text{-}RGO_{300}$ electrode exhibits the largest CV area, indicating the highest specific capacitance compared with the GO and the $T\text{-}RGO_{900}$. The high specific capacitance of $T\text{-}RGO_{300}$ results from the simultaneous contributions of the EDLCs and the pseudo-capacitance obtained from the oxygenated groups on the surface of GNSs.

Fig. 5B shows the CV curves of the GO, $T\text{-}RGO_{300}$ and the $T\text{-}RGO_{900}$ electrodes at the scan rate of 100 mV·s^{-1}. No obvious distortion in the CV curves are observed as the sweep rate increased to 100 mV·s^{-1}, suggesting a highly reversible system in the KOH electrolyte within the potential range employed. Generally, there are two key factors in determining the shape of CV curves: electrical conductivity of the electrode material (which affects the electronic transport performance of the electrode) and diffusive resistance of the electrolyte within electrode pores (which is related to the surface area and pore structure of the electrode material and affects the ion transport performance of the electrode). In this paper, due to the very poor electrical conductivity of GO materials, polarization of the GO electrode remains even at high sweep rate. The $T\text{-}RGO_{300}$ electrode has a small delay for the current to reach a horizontal value near the reversal of the potential sweep, reflecting a more significant diffusive resistance of the electrolyte in pores. In contrast, $T\text{-}RGO_{900}$ keeps a nearly rectangle at a high scan rate of 100 mV·s^{-1} because of its good electrical conductivity, high surface area and porous structure.

Fig. 6 shows the charge/discharge curves of the $T\text{-}RGO_{300}$ and the $T\text{-}RGO_{900}$ electrodes within a

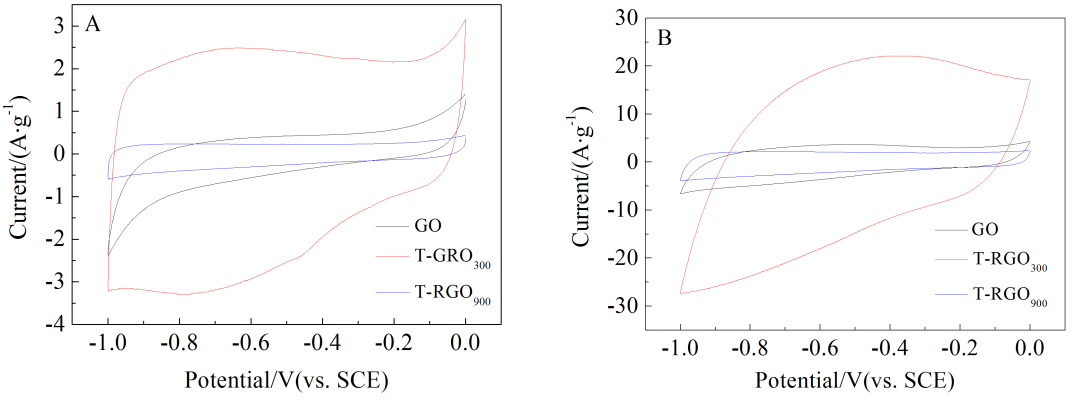

Fig. 5 CV curves of the GO, $T\text{-}RGO_{300}$ and the $T\text{-}RGO_{900}$ electrodes at sweep rate of 10 mV·s^{-1} (A) and 100 mV·s^{-1} (B) in KOH electrolyte

potential window of -1.0 to 0 V at a current density of 0.5 A·g^{-1}. The inset is the charge/discharge curve of the GO electrode within a potential window of -0.9 to 0 V at a current density of 2 A·g^{-1}. It can be observed that the shape of all the charge-discharge curves for the electrodes is closely linear and shows a typical triangle symmetrical distribution, displaying a good capacitive property. The specific capacitance value of the GO electrode according to formula (1) is 53 F·g^{-1}. After thermal reduction, the specific capacitance values of the T-RGO$_{300}$ and T-RGO$_{900}$ electrodes are 281 and 56 F·g^{-1}, respectively.

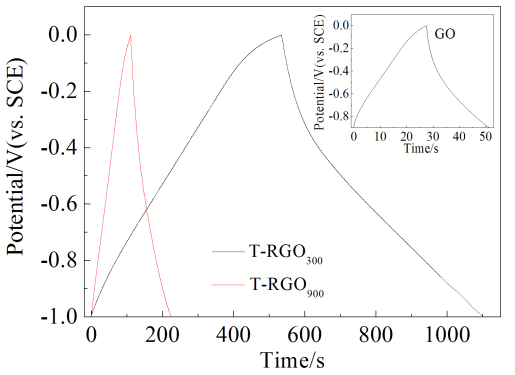

Fig. 6 The charge-discharge curves of the T-RGO$_{300}$ and the T-RGO$_{900}$ electrodes at a current density of 0.5 A·g^{-1} in KOH electrolyte (Inset is the charge/discharge curve of the GO electrode within a potential window of -0.9 to 0 V at a current density of 0.5 A·g^{-1})

It is pointed out that the GO sample which has the largest amount of oxygen-containing groups shows the lowest specific capacitance values due to its poor conductivity. This indicates that the good electrical conductivity is required for the electrode materials of supercapacitors. Moreover, the T-RGO$_{900}$ material with the highest specific surface area and pore volume shows a relatively low specific capacitance of only 56 F·g^{-1} due to its free of structural defects and few electrochemical active sites. However, the specific capacitance of T-RGO$_{300}$ with low specific surface area and abundant oxygen-containing groups is several times larger than that of the T-RGO$_{900}$. This indicates that the surface functional groups play more significant role than surface area in determining the supercapacitive performance of T-RGO.

Furthermore, the charge/discharge curves at different current densities of the GO, T-RGO$_{300}$ and T-RGO$_{900}$ electrodes were recorded. Fig. 7 reveals that the values of the specific capacitance for the all electrodes are strongly dependent on the current density. Owing to its poor conductivity, the specific capacitance of GO can not be measured successfully with the potential window of -1.0 to 0 V and current density of 0.5 A·g^{-1} or 1 A·g^{-1}(Fig. S1). In detail, the specific capacitance slightly decreases with the increase of the current density. Up to a relatively large current density of 10 A·g^{-1}, nearly 63%, 69% and 68% of the initial values remain for the GO, T-RGO$_{300}$ and T-RGO$_{900}$ electrodes, respectively. The result also shows that the T-RGO$_{300}$ and T-RGO$_{900}$ electrodes are favorable for the rapid diffusion and migration of electrolyte ions into the surfaces of graphene sheets during fast charge/discharge process, ensuring good rate capability.

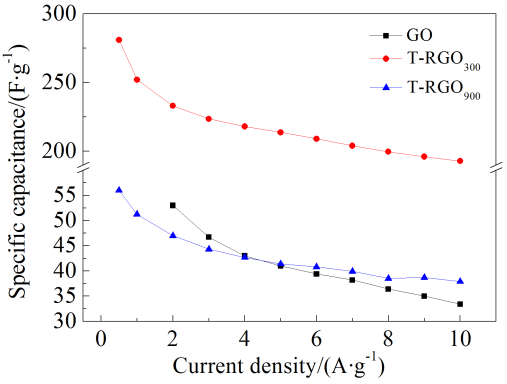

Fig. 7 Specific capacitance as a function of discharging current density for the GO, T-RGO$_{300}$ and T-RGO$_{900}$ electrodes

To further investigate the influence of thermal reduction temperature on the performance of the T-RGO, the supercapacitive performances of the T-RGO$_{200}$, T-RGO$_{300}$ and T-RGO$_{400}$ electrodes are also been systematically explored. Fig. 8A shows the CV curves of the T-RGO$_{200}$, T-RGO$_{300}$ and the T-RGO$_{400}$ electrodes at the scan rates of 10 mV·s^{-1} and 100 mV·s^{-1} between -1.0 and 0 V in 2 mol·L^{-1} KOH

aqueous electrolyte. It is clear that the T-RGO$_{200}$ electrode exhibits the largest CV area, indicating the highest specific capacitance compared with the T-RGO$_{300}$ and the T-RGO$_{400}$. It is mainly due to that the T-RGO$_{200}$ contains more residual oxygenate groups than T-RGO$_{300}$ and T-RGO$_{400}$. Fig. 8B shows the CV curves of the T-RGO$_{200}$, T-RGO$_{300}$ and T-RGO$_{200}$ electrodes at a high scan rate of 100 mV·s^{-1}. Owing to its poor conductivity, an obvious distortion in the CV curve of T-RGO$_{200}$ is observed, while the CV curves of T-RGO$_{300}$ and T-RGO$_{400}$ still keep nearly rectangle, and T-RGO$_{300}$ has the larger CV area. As shown in Fig. 8C, the specific capacitance values of the T-RGO$_{200}$, T-RGO$_{300}$ and T-RGO$_{400}$ electrodes are 288, 281 and 159 F·g^{-1}, respectively, at the discharge current density of 0.5 A·g^{-1}. However, when the discharge current density increases up to 10 A·g^{-1}, nearly 59% and 69 % of the initial values are remained for the T-RGO$_{200}$ and T-RGO$_{300}$ electrodes, respectively. Compared with T-RGO$_{200}$, T-RGO$_{300}$ electrode has a higher capacitance retention at large current density. Taking its high capacitance, low energy-consumption and large current stability into consideration, thermal reduction at 300 ℃ is the best choice to obtain T-RGO as a supercapacitor electrode material.

The complex plane plots of the AC impedance spectra for the T-RGO$_{200}$, T-RGO$_{300}$ and T-RGO$_{400}$ electrodes are shown in Fig. 8D. Internal resistance (which is equal to R_b, including the intrinsic resistance of the electroactive material, the resistance of KOH aqueous solution and the contact resistance at the interface between the electrode and current collector) can be obtained from the crossover point of the high frequency with the real part of the impedance of the Nyquist plots. The R_b values are estimated to be 0.65, 0.46 and 0.44 Ω for the T-RGO$_{200}$, T-RGO$_{300}$

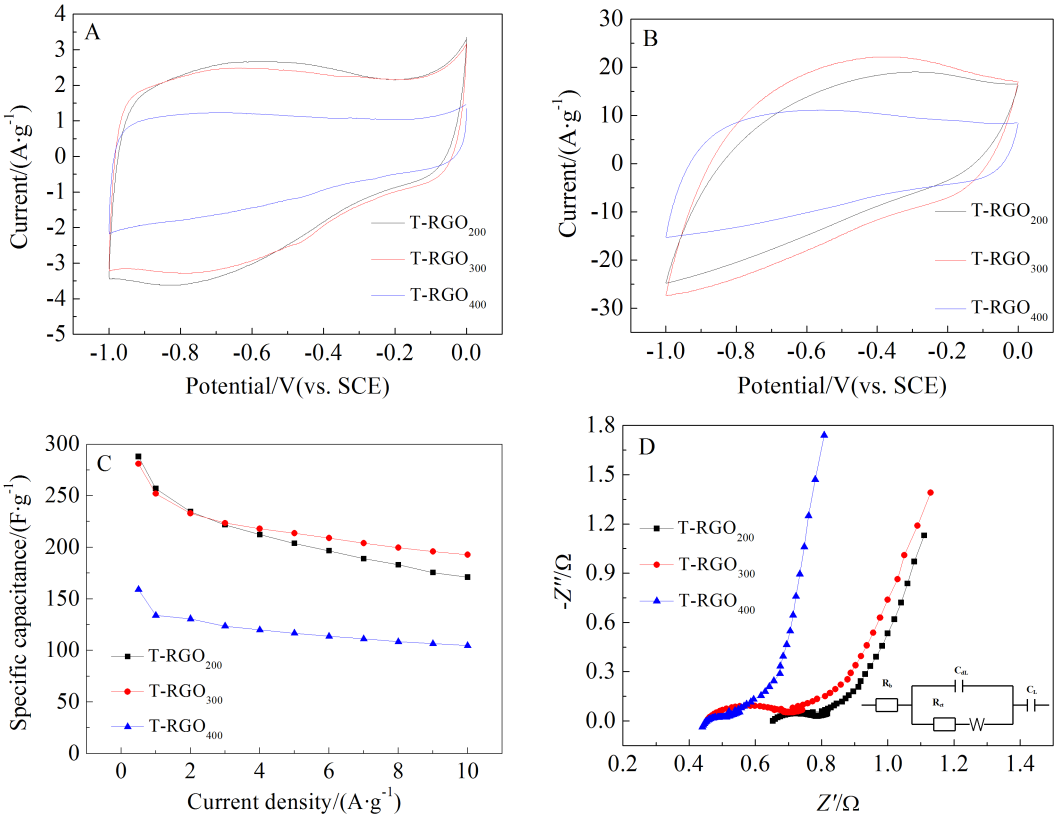

Fig. 8 CV curves of the T-RGO$_{200}$, T-RGO$_{300}$ and T-RGO$_{400}$ electrodes at sweep rates of 10 mV·s^{-1} (A) and 100 mV·s^{-1} (B) in KOH electrolyte; C. The specific capacitance as a function of discharging current density for the T-RGO$_{200}$, T-RGO$_{300}$ and T-RGO$_{400}$ electrodes; D. Complex-plane impedance plots of the T-RGO$_{200}$, T-RGO$_{300}$ and T-RGO$_{400}$ electrodes (The inset is an equivalent circuit)

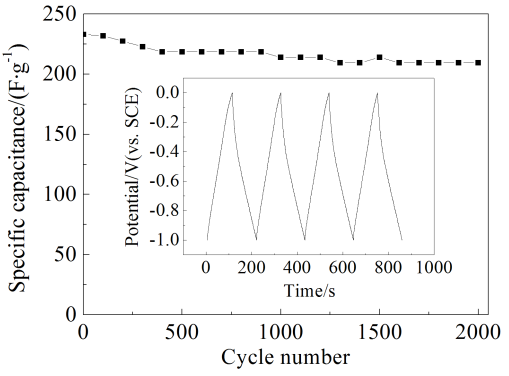

Fig. 9 Cycle life of the T-RGO$_{300}$ electrode at the current density of 2 A·g^{-1} in KOH electrolyte

and T-RGO$_{900}$ electrodes, respectively. The semicircle in the high frequency range associates with the surface properties of the porous electrode, which corresponds to the faradic charge transfer resistance (R_{ct}). At the lower frequencies, a straight sloping line represents the diffusive resistance (warburg impendence, W) of the electrolyte in electrode pores and the proton diffusion in host material. As seen in Fig. 8D, the conductive performances increase in the sequence of T-RGO$_{200}$ < T-RGO$_{300}$ < T-RGO$_{400}$. These observations are strongly correlated with the result of large current stability test (Fig. 8C). The results of complex plane plots and Tab. 2 indicate that the electrochemical conductive performances are enhanced significantly with the increase in the temperature of thermal reduction.

The cycle life of the T-RGO$_{300}$ electrode was monitored by a chronopotentiometry measurement at 2 A·g^{-1} in 2 mol·L^{-1} KOH electrolyte. As shown in Fig. 9, the specific capacitance of the T-RGO$_{300}$ electrode decreases gradually with the increase of the cycle number. After a continuous 2000 cycling, the specific capacitance remains 90% of the initial value. This demonstrates that the oxygen functional groups in the surface of T-RGO$_{300}$ are relatively stable for electrochemical systems, and within the voltage window -1.0 to 0 V, the repeating charge-discharge behaviours seem not to induce a significant structural change for the T-RGO$_{300}$ electrode. The long-term stability implies that the T-RGO$_{300}$ is an excellent electrode material for supercapacitors.

3 Conclusions

An investigation of the supercapacitance of T-RGO materials was carried out. Three aspects of surface area, electrical conductivity and surface functional groups are discussed. The result shows that it is not necessary for T-RGO with higher specific surface area and better electrical conductivity to achieve larger specific capacitance. The T-RGO$_{300}$ with a low specific surface area of 18.8 m^2·g^{-1} possesses the maximum specific capacitance of 281 F·g^{-1}. It indicates that a certain amount of oxygen-containing functional groups on T-RGO surfaces play a very important role in determining the electrochemical capacitance. Thus, it probably gives a new insight for designing and synthesizing graphene-based electrode materials for supercapacitors and other energy-storage devices.

Supporting Information Available

The supporting information is available free of charge via the internet at http://electrochem.xmu.edu.cn.

References:

[1] Winter M, Brodd R J. What are batteries, fuel cells, and supercapacitors[J]. Chemical Reviews, 2004, 104(10): 4245-4269.

[2] Simon P, Gogotsi Y. Materials for electrochemical capacitors[J]. Nature materials, 2008, 7(11): 845-854.

[3] Aboutalebi S H, Chidembo A T, Salari M, et al. Comparison of GO, GO/MWCNTs composite and MWCNTs as potential electrode materials for supercapacitors[J]. Energy & Environmental Science, 2011, 4(5): 1855-1865.

[4] Wu Z S, Wang D W, Ren W C, et al. Anchoring hydrous RuO_2 on graphene sheets for high-performance electrochemical capacitors[J]. Advanced Functional Materials, 2010, 20(20): 3595-3602.

[5] Lang J W, Kong L B, Wu W J, et al. Facile approach to prepare loose-packed NiO nano-flakes materials for supercapacitors[J]. Chemical Communications, 2008, (35): 4213-4215.

[6] Zhu Y W, Murali S, Stoller D S, et al. Carbon-based supercapacitors produced by activation of graphene[J]. Science, 2011, 332(6037): 1537-1541.

[7] Frackowiak E. Carbon materials for supercapacitor appli cation[J]. Physical Chemistry Chemical Physics, 2007, 9 (15): 1774-1785

[8] Zhu Y W, Murali S, Cai W W, et al. Graphene and graphene oxide: Synthesis, properties, and applications[J]. Advanced Materials, 2010, 22(35): 3906-3924.

[9] Hou J B, Shao Y Y, Ellis M W, et al. Graphene-based electrochemical energy conversion and storage: Fuel cells, supercapacitors and lithium ion batteries[J]. Physical Chemistry Chemical Physics, 2011, 13(34): 15384-15402.

[10] Yan J, Wei T, Shao B, et al. Electrochemical properties of graphene nanosheet/carbon black composites as electrodes for supercapacitors [J]. Carbon, 2010, 48 (6): 1731-1737.

[11] Hulicova-Jurcakova D, Seredych M, Lu G Q, et al. Combined effect of nitrogen-and oxygen-containing functional groups of microporous activated carbon on its electrochemical performance in supercapacitors [J]. Advanced Functional Materials, 2009, 19(3): 438-447.

[12] Khomenko V, Raymundo-Pinero E, Béguin F. A new type of high energy asymmetric capacitor with nanoporous carbon electrodes in aqueous electrolyte [J]. Journal of Power Sources, 2010, 195(13): 4234-4241.

[13] Stoller D M, Park S, Zhu Y W, et al. Graphene-based ultracapacitors[J]. Nano Letters, 2008, 8(10): 3498-3502.

[14] Du Q L, Zheng M B, Zhang L F, et al. Preparation of functionalized graphene sheets by a low-temperature thermal exfoliation approach and their electrochemical supercapacitive behaviors[J]. Electrochimica Acta, 2010, 55(12): 3897-3903.

[15] Chen J T, Zhang G A, Luo B M, et al. Surface amorphization and deoxygenation of graphene oxide paper by Ti ion implantation[J]. Carbon, 2011, 49(9): 3141-3147.

[16] Lang J W, Yan X B, Xue Q J. Facile preparation and electrochemical characterization of cobalt oxide/multi-walled carbon nanotube composites for supercapacitors [J]. Journal of Power Sources, 2011, 196(18): 841-7846.

[17] Lv W, Tang D M, He Y B, et al. Low-temperature exfoliated graphenes: Vacuum-promoted exfoliation and electrochemical energy storage[J]. ACS Nano, 2009, 3(11): 3730-3736.

影响热还原氧化石墨烯超级电容器性能的因素比较

肖 鹏[1,2], 王大辉[1*], 郎俊伟[2*]

(1. 兰州理工大学材料科学与工程学院, 甘肃 兰州 730050;
2. 中国科学院兰州化学物理研究所, 清洁能源化学与材料实验室, 甘肃 兰州 730000)

摘要: 通过改进的 Hummer 法制得氧化石墨烯, 并在不同温度的氩气气氛中还原得到一系列热还原氧化石墨烯(T-RGO). 电化学测试表明,T-RGO 作为超级电容器电极材料时,良好的导电性是必需的,但石墨烯表面含氧官能团对其电容性能的影响要远大于导电性和比表面积的影响. 900 ℃ 还原的 T-RGO 比表面积为 314 $m^2 \cdot g^{-1}$, 电导率为 2421 $S \cdot m^{-1}$,但其容量只有 56 $F \cdot g^{-1}$. 而 300 ℃ 还原的 T-RGO 比表面积为 18.8 $m^2 \cdot g^{-1}$,电导率为 574 $S \cdot m^{-1}$,其容量却达到 281 $F \cdot g^{-1}$. 材料表征分析表明,300 ℃ 还原的石墨烯之所以有更高的电容,是因为除双电层电容外,更多的是由其表面含氧官能团提供的赝电容,这使作者以后在设计制备超级电容器等储能设备用石墨烯基电极材料时更加有针对性.

关键词: 石墨烯; 赝电容; 超级电容器; 表面官能团; 热还原